Caught Bending the A-Rule: Crystal Structures of Translesion DNA Synthesis with a Non-Natural Nucleotide†

Karl E. Zahn,‡ Hassan Belrhali,§ Susan S. Wallace,*,‡ and Sylvie Doublié*,‡

Department of Microbiology and Molecular Genetics, University of Vermont, Burlington, Vermont 05405, and European Molecular Biology Laboratory, 6 rue Jules Horowitz, BP 181, F-38042 Grenoble Cédex 9, France

Received May 9, 2007; Revised Manuscript Received June 15, 2007

ABSTRACT: Damage to DNA involving excision of the nucleobase at the N-glycosidic bond forms abasic sites. If a nucleotide becomes incorporated opposite an unrepaired abasic site during DNA synthesis, most B family polymerases obey the A-rule and preferentially incorporate dAMP without instruction from the template. In addition to being potentially mutagenic, abasic sites provide strong blocks to DNA synthesis. A previous crystal structure of an exonuclease deficient variant of the replicative B family DNA polymerase from bacteriophage RB69 (RB69 gp43 exo−) illustrated these properties, showing that the polymerase failed to translocate the DNA following insertion of dAMP opposite an abasic site. We examine four new structures depicting several steps of translesion DNA synthesis by RB69 gp43 exo−, employing a non-natural purine triphosphate analogue, 5-nitro-1-indolyl-2′-deoxyriboside-5′-triphosphate (5-NITP), that is incorporated more efficiently than dAMP opposite abasic sites. Our structures indicate that a dipole-induced dipole stacking interaction between the 5-nitro group and base 3′ to the templating lesion explains the enhanced kinetics of 5-NITP. As with dAMP, the DNA fails to translocate following insertion of 5-NIMP, although distortions at the nascent primer terminus contribute less than previously thought in inducing the stall, given that 5-NIMP preserves relatively undistorted geometry at the insertion site following phosphoryl transfer. An open ternary configuration, novel in B family polymerases, reveals an initial template independent binding of 5-NITP adjacent to the active site of the open polymerase, suggesting that closure of the fingers domain shuttles the nucleotide to the active site while testing the substrate against the template.

Replicative DNA polymerases preserve the integrity of the genome by catalyzing the template directed extension of a nucleic acid primer with exquisite accuracy. The fidelity of DNA synthesis depends on the necessarily variable substrate specificity of the replicative polymerase, whose task is to incorporate the nucleotide complementary to the ever changing templating base. In the absence of coding information due to nucleobase loss, most replicative polymerases obey the A-rule, preferentially incorporating dAMP in the primer strand opposite these nontemplating DNA lesions (abasic or AP sites), although incorporation of dGMP also occurs to a lesser extent (*1*−*5*).

Abasic sites arise at high steady-state levels, forming 2000−10000 potentially mutagenic lesions in a single human cell each day (*6*). While spontaneous depurination provides the primary mechanism, hydroxyl radical attack at the C1′ carbon of deoxyribose sugars also produces these lesions (*7*). Furthermore, abasic sites occur as intermediates of the base excision repair pathway, where N-glycosylases cleave damaged nucleobases during maintenance of DNA (*8*).

Abasic sites provide strong blocks to DNA synthesis that can preclude replication of the genome, as evinced by the lethality to some cells of transfecting DNAs containing abasic sites (*9*, *10*). Following insertion of dAMP opposite an abasic site, a replicative polymerase bearing accessory exonuclease proofreading activity usually edits the inserted base, stalling in unproductive rounds of incorporation and excision that cease progression of the replication fork (*4*). A recent crystal structure (*11*) caught a 3′-5′ exonuclease deficient variant of the high fidelity DNA polymerase from bacteriophage RB69 (RB69 gp43 exo−) inserting dAMP opposite 2′-deoxyfuranoside (furan[1]), a synthetic abasic site analogue (*5*). This crystal, referred to as F_{18}•dAMP,[2] contained four conformers of the enzyme per asymmetric unit, where each represented an intermediate state during migration of the primer DNA strand from the polymerase to the exonuclease active site.

† This work was supported by a National Institutes of Health grant (CA52040) to S.S.W. GM/CA CAT has been funded in whole or in part with Federal funds from the National Cancer Institute (Y1-CO-1020) and the National Institute of General Medical Science (Y1-GM-1104). Use of the Advanced Photon Source was supported by the U.S. Department of Energy, Basic Energy Sciences, Office of Science, under Contract No. DE-AC02-06CH11357.

* To whom correspondence should be addressed. S.D.: tel, (802) 656-9531; fax, (802) 656-8749; e-mail, sdoublie@uvm.edu. S.S.W.: tel, (802) 656-2164; fax, (802) 656-8749; e-mail, swallace@uvm.edu.

‡ University of Vermont.

§ European Molecular Biology Laboratory.

[1] Abbreviations: furan, 2′-deoxy-furanoside; 5-NITP, 5-nitro-1-indolyl-2′-deoxyriboside-5′-triphosphate; dPTP, pyrene-2′-deoxynucleoside-5′-triphosphate; Ind-TP, indolyl-2′-deoxyriboside-5′-triphosphate; RB69 gp43 exo−, exonuclease deficient bacteriophage RB69 DNA polymerase (D222A/D327A); PEG 2000-MME, polyethylene glycol 2000 monomethylether; PEG 20 000, polyethylene glycol 20 000.

[2] For all complexes described in this manuscript, the number in subscript refers to the number of bases in the template DNA strand.

10.1021/bi7008807 CCC: $37.00
Published on Web 08/24/2007

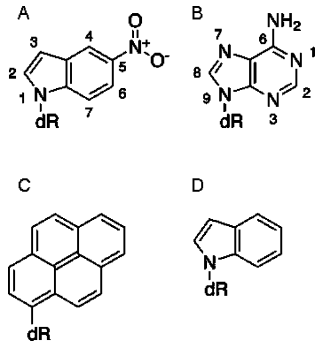

FIGURE 1: Chemical structures of 2′-deoxynucleoside triphosphates referenced in this work. A. 5-nitro-1-indolyl-2′-deoxyriboside-5′-triphosphate (5-NITP). B. 2′-deoxyadenosine-5′-triphosphate (dATP). C. pyrene-2′-deoxynucleoside-5′-triphosphate (dPTP). D. indolyl-2′-deoxyriboside-5′-triphosphate (Ind-TP).

These complexes illustrated that proofreading of dAMP coincides with a loss of minor groove contacts between the enzyme and DNA, with the associated stall allowing the switch of the primer strand from the polymerase to the exonuclease active site.

To further elucidate the mechanism underpinning the A-rule, the biochemical properties of several non-natural purine triphosphate analogues were examined (*12*−*15*). 5-Nitro-1-indolyl-2′-deoxyriboside-5′-triphosphate (5-NITP, Figure 1A) demonstrated a 1000-fold greater incorporation efficiency over that of dATP (Figure 1B) when inserted opposite furan by B family (polymerase α-like) DNA polymerases, such as those from RB69 or T4 (*15*). This base analogue pairs with all other natural bases (*16*), stabilizing DNA and remaining intrahelical (*17*) except in long repeated stretches where hairpin structures result, and was originally synthesized for use in degenerate PCR primers as a potentially universal nucleobase (*18*). While incorporation of 5-NIMP opposite undamaged templates by RB69 gp43 exo− progresses more slowly than is the case with furan templates, the product is never extendable, which shows that 5-NITP is a chain terminator of DNA synthesis (*13*).

Currently, the A-rule for replicative DNA polymerases remains under study. A steric matching mechanism speculates that hydrogen bonding carries less importance for specificity of incorporation than precise geometric criterion selecting natural base pairs in the polymerase active site (*19*, *20*), although this model may not apply to B family polymerases (*21*). Steric matching identifies pyrene-2′-deoxynucleoside-5′-triphosphate (dPTP, Figure 1C) as an ideal complement opposite an abasic site, since pyrene itself is nearly as large as a Watson−Crick base pair (*22*). While dPMP is inserted opposite AP sites with 100-fold greater efficiency than dAMP (*12*), the efficiency of pyrene does not approach that of 5-nitroindole, which is much smaller in size. Incorporation of hydrophobic bases lacking functional groups for hydrogen bonding to natural bases also occurs without need for desolvation, since these bases do not hydrogen bond with water. However, hydrophobicity alone cannot account for preferential incorporation of dAMP over other natural nucleotides opposite AP sites. Indolyl-2′-deoxyriboside-5′-triphosphate (Ind-TP; Figure 1D), though much more hydrophobic, is incorporated opposite furan with efficiency similar to that of dAMP (*12*). In general, neither steric constraints nor hydrophobicity appears to be the driving force behind the insertion step of DNA synthesis by B family polymerases, although the former consideration may be important for subsequent extension of a base pair (*21*, *23*).

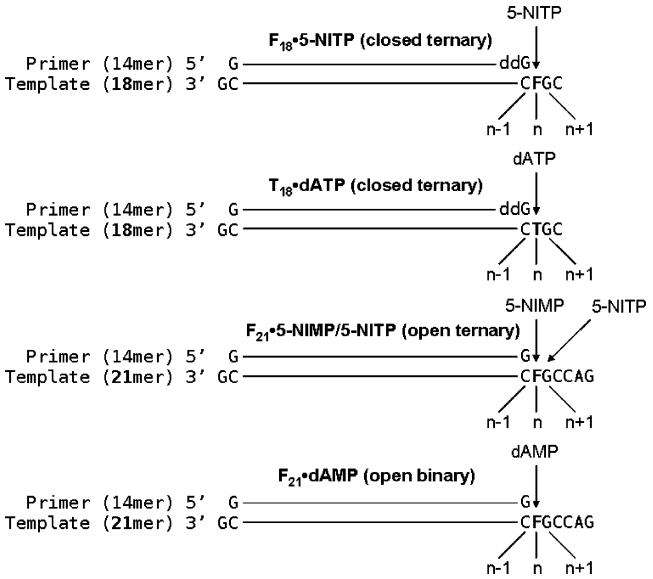

FIGURE 2: Constructs of refined models in this work. The *n* position refers to the polymerase active site, while the $n + 1$ position is one base in the template 5′ direction and the $n - 1$ position is one base pair in the other direction, such that the polymerase moves in the positive direction. The first letter in the construct name refers to the base in the templating position, or template *n* position, and the subscript indicates the number of bases in the template. The open or closed descriptor signifies the conformational state of the fingers domain. Binary complexes are between RB69 gp43 exo− and double stranded DNA, containing no noncovalently incorporated nucleoside triphosphates. Ternary complexes contain RB69 gp43 exo−, double stranded DNA, and a bound or coordinated nucleoside triphosphate. The dGMP overhang at the template 3′ end is needed to ensure desired crystal packing.

The favorable kinetics of inserting 5-NITP opposite AP sites by B family polymerases, paired with the capacity of RB69 gp43 exo− to form crystals in complex with DNA containing furan, creates an ideal crystallographic tool. We set out to apply these attributes, capturing four crystal structures (Figure 2) of transient complexes that compare incorporation of dATP and 5-NITP opposite furan by RB69 gp43 exo−. A closed ternary complex shows formation of a Watson−Crick T•A base pair directly before phosphoryl transfer (T_{18}•dATP). We also present an untranslocated binary complex orienting dAMP across from furan after chemical incorporation into the primer DNA strand (F_{21}•dAMP). A second closed ternary complex describes 5-NITP coordinated in the polymerase active site opposite furan (F_{18}•5-NITP). The subsequent open ternary complex depicts both the incorporated 5-NIMP in an untranslocated state with furan in templating position following the chemical step of catalysis, and a 5-NITP molecule bound to the fingers domain adjacent to the active site (F_{21}•5-NIMP/5-NITP). This complex describes a binding event prior to testing of the substrate, which is a novel observation in B family DNA polymerases, before the dNTP encounters the template in the polymerase active site.

EXPERIMENTAL PROCEDURES

Materials. DNA primers and templates were synthesized by Midland Certified and gel purified. 5-NITP was purchased

from Trilink Biotech, while other nucleotides were from Invitrogen or USB. Polyethylene glycol 2000 monomethylether (PEG 2000-MME) and polyethylene glycol 20 000 (PEG 20 000) were purchased from Hampton Research. All other chemicals were from Fisher or Sigma.

Protein Expression. Untagged exonuclease deficient RB69 gp43 exo− (D222A/D327A) was expressed and purified according to previously published protocols (*11*). A selenomethionyl variant of the same enzyme was expressed via the methionine pathway inhibition method (*24*) and purified using a protocol similar to that of the native enzyme (*11*).

Crystallization. All double stranded oligonucleotides used for crystallization carried a dGMP overhang on the template 3′ end that binds in a pocket of the N-terminal domain of an adjacent polymerase/DNA complex to stabilize the crystal lattices, which was shown to be critical for formation of diffraction quality crystals (*25*). F_{18}•5-NITP, F_{21}•5-NIMP/5-NITP, and F_{21}•dAMP utilize furan as a synthetic abasic site analogue, which is an established method (*5*, *11*, *26*).

Ternary Complexes. 18-Mer templates (5′-CG(F)CTTATGACAGCCGCG and 5′-CGTCTTATGACAGCCGCG, where (F) represents a furan) were annealed to a complementary 13-mer primer (5′-GCGGCTGTCATAA) for use in crystallization trials. Annealing of these oligos placed dCMP in the templating position, such that the adjacent dTMP or furan was located at the $n + 1$ template position. RB69 gp43 exo− (100 μM) was incubated for 30 min at room temperature with template•primer DNA (120 μM) and ddGTP (1 mM) in a buffered reaction solution containing $MgCl_2$ (6 mM), dithiothreitol (2 mM), Hepes-NaOH pH 7.5 (10 mM), NaCl (33 mM), chain terminating the primer and moving dTMP or furan to templating position. 5-NITP was added to a final concentration of 13 mM to the solution containing the furan modified template, whereas an equal concentration of dATP was added to the solution with the unmodified template. Hanging crystallization drops were made by mixing 0.5 μL of reaction solution with 0.5 μL of a reservoir solution of PEG 20 000 (2−3% (w/v)), CH_3COONa pH 5.0 (100 mM), $(CH_3COO)_2Mg$ (100 mM), Tris-HCl pH 7.0−7.5 (100 mM), beta-mercaptoethanol (2 mM), and glycerol (0.1% (v/v)), and equilibrated against 1 mL of the reservoir solution for 3 days at 20 °C. Orthorhombic ($P2_12_12_1$) crystals of the F_{18}•5-NITP complex grew to a maximum size of 180 μm × 60 μm × 60 μm, whereas the T_{18}•dATP complex produced slightly larger crystals in the same space group. Cell parameters were similar for both complexes, and in keeping with other published ternary complexes of RB69 gp43 exo− (*25*, *27*) (Table 1).

Binary Complexes. A 21-mer template (5′-GACCG(F)-CTTATGACAGCCGCG) was annealed to a complementary 14-mer primer (5′-GCGGCTGTCATAAG), placing furan in templating position. Two reaction solutions were then prepared on ice, one of RB69 gp43 exo− (100 μM), DNA template•primer (150 μM), 5-NITP (2 mM), $MgCl_2$ (6 mM), dithiothreitol (2 mM), Hepes-NaOH pH 7.5 (100 mM), and NaCl (33 mM). The other solution was identical, except that dATP (2 mM) and the selenomethionyl variant were used instead of 5-NITP and the natural enzyme. The selenomethionyl variant often produces larger, better diffracting crystals (*28*), and was employed only for this reason. Hanging drops were set up immediately by mixing 0.5 μL reaction solution with 0.5 μL of a reservoir solution containing PEG 2000-MME (7−10% (w/v)), CH_3COONa (100 mM), $MgSO_4$ (150 mM), Hepes-NaOH pH 7.0 (100 mM), beta-mercaptoethanol (2 mM), and glycerol (10% (v/v)). These drops equilibrated at 20 °C against 1 mL reservoirs for 5 days, after which monoclinic crystals ($P2_1$) were obtained with dimensions of 140 μm × 100 μm × 100 μm.

Cryoprotection. All crystals were cryoprotected by increasing the concentration of PEG by 1% (w/v) and bringing the glycerol concentration up to 18% (v/v) directly in the crystallization drop. After allowing approximately 2 min for diffusion of the cryoprotectant, crystals were mounted in micro loops and plunged into liquid N_2.

Data Collection. X-ray diffraction data were collected under cryocooled conditions (100 K) at high-intensity synchrotron sources. Data for ternary complexes were collected at the European Synchrotron Radiation Facility (ESRF) beam line BM14 at $\lambda = 0.873$ Å on a MARMOSAIC 225mm CCD detector, whereas binary complex data collection occurred at the Advanced Photon Source (APS) beam line ID23-D with $\lambda = 0.979$ Å on a MAR m300 CCD detector. Except for the binary complex with dAMP, which was processed with HKL2000, all other intensities were integrated in Denzo (*29*). All data sets were scaled and merged with Scalepack (*29*) (Table 1).

Structure Solution. RB69 gp43 exo− models 1IG9 (*25*) and 2P5O (*11*) provided initial solutions for the ternary and binary complexes, respectively. These coordinates were refined with CNS (*30*) by rigid body refinement, fitting protein domains (*31*) under cross validation by test sets extracted from the parent structures. Rounds of manual building in COOT (*32*) followed simulated annealing and energy minimization in CNS under relaxed NCS restraints between protein domains. Refmac (*33*) provided the final idealization and refinement of coordinates, which were validated in Procheck (*34*). Ramachandran plots of torsion angles placed each residue in allowed regions except T622, which is an expected property of this residue that neighbors the catalytic aspartate D623 (*11*, *25*, *27*, *28*, *35*). Due to resolution constraints, the nitro group of 5-nitroindole was restrained to the plane of the indole rings during refinement, although a small molecule structure depicts the oxygen atoms 5° skew (CCDC ID code: 100476) (*18*). All 5-NITP molecules bound to the F_{21}•5-NIMP/5-NITP open ternary complexes were assigned an occupancy of 0.7. While the resolution of this data set does not allow refinement of occupancy, an occupancy of 0.7 was deemed a valid estimate (*36*), bringing the average temperature factors of these 5-NITP molecules into agreement with the overall average temperature factor for the F_{21}•5-NIMP/5-NITP structure (Table 1). The final coordinate files employ naming conventions identical to those of parent structures for both protein and DNA molecule identification. Therefore, in both the open ternary complex F_{21}•5-NIMP/5-NITP and the open binary complex F_{21}•dAMP, where the asymmetric unit contains four molecules (MolA−D), the DNA in MolA and MolC remains in the polymerase active site. MolB holds the DNA primer in the exonuclease active site. MolD is the most disordered molecule in the structures, with the weakest overall electron density. Discussion in this manuscript of the open complexes (F_{18}•dAMP, F_{21}•dAMP, and F_{21}•5-NIMP/5-NITP) pertains only to MolC, the polymerase conformer built into strongest overall electron density. Since closed ternary complexes

Table 1: Crystallographic Statistic and Structure Refinement Table. All Data Sets Were Collected from a Single Crystal. Statistics for the Highest-resolution Shells Are Shown in Parentheses.

	F_{18}•5-NITP closed ternary complex	T_{18}•dATP closed ternary complex	F_{21}•5-NIMP/5-NITP open ternary complex	F_{21}•dAMP open binary complex
PDB ID code	2OZM	2OZS	2OYQ	2P5G
beamline	ESRF BM14	ESRF BM14	APS ID23-D	APS ID23-D
wavelength (Å)	0.873	0.873	0.979	0.979
contents of asymmetric unit	1 polymerase/DNA complex	1 polymerase/DNA complex	4 polymerase/DNA complexes	4 polymerase/DNA complexes
data collection				
space group	$P2_12_12_1$	$P2_12_12_1$	$P2_1$	$P2_1$
cell dimensions				
a, *b*, *c* (Å)	81.2, 117.5, 126.1	81.3, 117.8, 129.1	132.6, 123.5, 164.3	132.4, 122.8, 164.8
α, *β*, *γ* (deg)	90.0, 90.0, 90.0	90.0, 90.0, 90.0	90.0, 96.2, 90.0	90.0, 96.3, 90.0
resolution (Å)	30−2.80 (2.90−2.80)	50−2.75 (2.85−2.75)	30−2.86 (2.96−2.86)	50−2.80 (2.90−2.80)
R_{merge} (%)	14.4 (37.4)	14.8 (34.1)	8.7 (60.1)	8.5 (40.2)
$I/\sigma I$	8.7 (2.9)	8.6 (2.7)	14.4 (2.0)	11.3 (2.6)
completeness (%)	94.7 (71.6)	94.9 (73.1)	99.6 (97.3)	98.5 (87.7)
redundancy	4.5 (3.0)	4.1 (3.7)	4.4 (3.7)	3.4 (3.2)
refinement				
resolution (Å)	30−2.80	30−2.75	30−2.86	30.0−2.80
no. of reflections	26082	27781	100166	101465
R_{work}/R_{free} (%)	20.4/26.8	20.6/26.6	22.8/29.4	23.4/29.5
rms deviations				
bond lengths (Å)	0.007	0.010	0.007	0.007
bond angles (deg)	1.072	1.307	1.101	1.062
no. of atoms	8402	8314	28889	29179
protein	7328	7350	A 6877	A 7143
			B 6045	B 6036
			C 7150	C 7113
			D 5688	D 6148
DNA	641	650	A 624	A 611
			B 510	B 531
			C 705	C 703
			D 509	D 491
5-NITP	32	none	128	none
dATP	none	30	none	none
Mg^{2+}	1	1	2	none
water	400	283	651	403
B-factors (Å^2)				
average	63.8	59.2	74.8	73.9
protein	65.1	59.9	A 56.1	A 59.2
			B 70.9	B 72.1
			C 66.4	C 64.3
			D 123.3	D 116.5
DNA	59.2	55.6	A 96.8	A 81.7
			B 119.0	B 106.8
			C 70.8	C 67.7
			D 95.9	D 109.3
5-NITP	39.7	none	77.0	none
dATP	none	35.0	none	none
Mg^{2+}	42.7	44.3	75.5	none
water	59.0	55.0	55.6	57.5

contain only a single protein molecule per asymmetric unit, discussion describes that entire asymmetric unit.

All three-dimensional diagrams of proteins and nucleic acids were generated in PyMOL (*37*). The structural superpositions were created by aligning the α-carbons of the palm domain residues (383−468 and 573−729).

RESULTS

5-NITP Inserted Opposite an Abasic Site Stacks with the Template Strand. Ternary complexes of RB69 gp43 exo− were captured by dideoxy chain terminating the template•primer pair enzymatically prior to providing the polymerase with the desired incoming nucleoside triphosphate (*38*, *39*). This technique allowed for crystallization of both a closed complex of 5-NITP coordinated opposite an abasic site (F_{18}•5-NITP, Figure 2) and a natural closed complex with dATP opposite a templating dTMP (T_{18}•dATP, Figure 2). Structures were solved at 2.80 and 2.75 Å, respectively, resolving a single Mg^{2+} ion coordinated by the catalytic aspartates D411 and D623, the oxygen from the carbonyl group of L412, and three nonbridging oxygens of the triphosphate tail at an average distance in each structure of 2.1−2.2 Å. Mg^{2+} is the metal most likely required for physiological activity (*40*) and thus provided optimal coordination geometry with the enzyme and triphosphate, allowing us to visualize the orientation of 5-NITP opposite an abasic site directly prior to phosphoryl transfer (Figure 3): 5-NITP is intrahelical and the distance between the indole rings and the adjacent base is about 3.4 Å, an interplanar spacing characteristic of B-form DNA. The nitro moiety extends into the void left by the

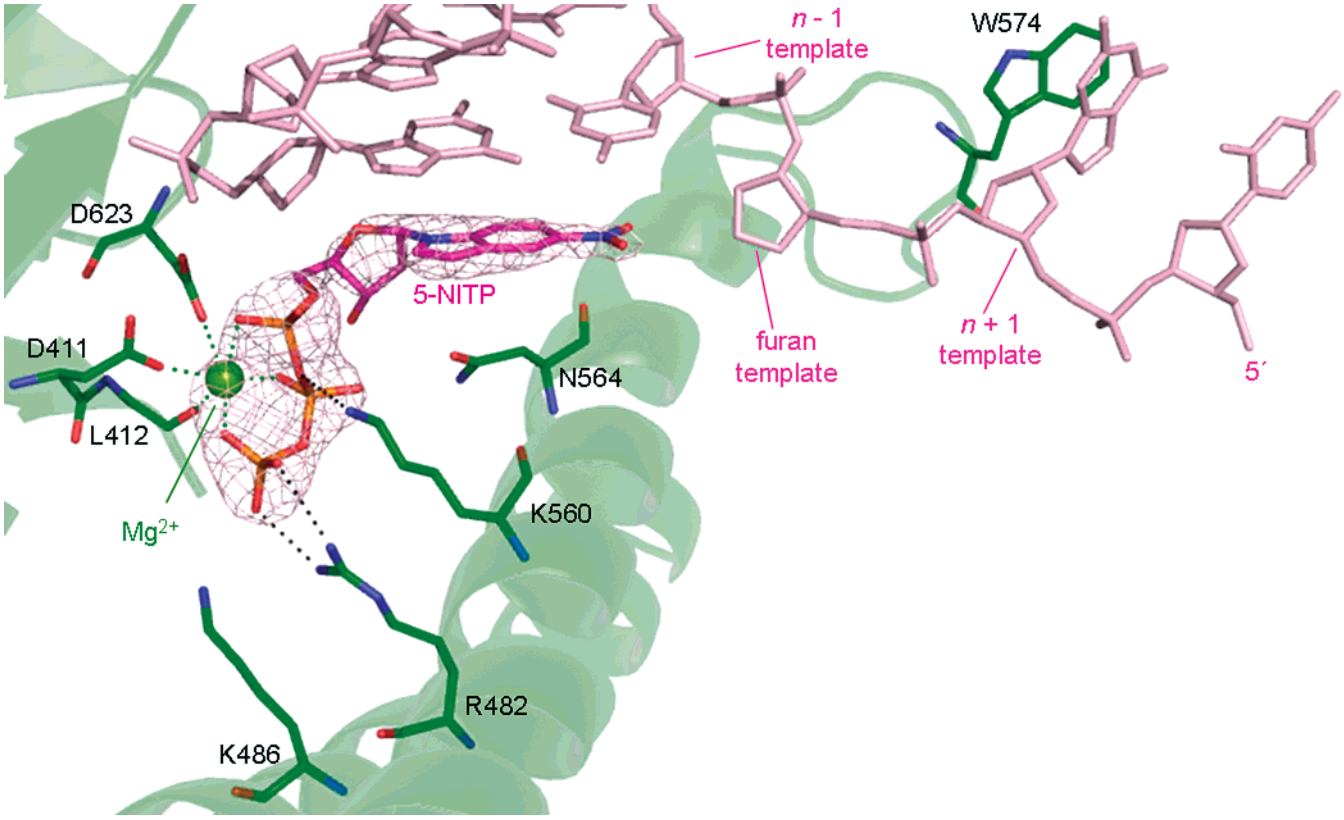

FIGURE 3: F_{18}•5-NITP closed ternary complex. A 2.8 Å simulated annealing omit map contoured at 5σ shows 5-NITP bond in the polymerase active site opposite furan in the closed ternary complex. Coordination interactions with Mg^{2+} are shown as green dashes, whereas hydrogen bonds are depicted in black. The $n + 1$ template base stacks on W574.

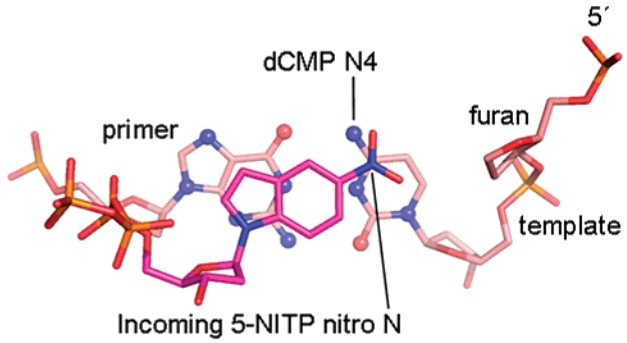

FIGURE 4: Close-up of 5-NITP in the F_{18}•5-NITP closed ternary complex. The nitro moiety of the incoming 5-NITP molecule stacks with the $n - 1$ template base. This base stacking occurs under a dCMP•dGMP pair, where the nitro extends into the void at the abasic site to overlap with the C4 of dCMP in this view.

abasic site and stacks under the template strand without tight steric constraints, leaving a gap of approximately 3.6 Å between the nitro moiety and the furan. The nitro N resides directly under the C4 of the cytosine 3′ to the abasic site at the $n - 1$ position (Figure 4). When compared to T_{18}•dATP, we observe that the indole rings are superimposable over the purine in the normal T•A base pair (Figure 5A), showing that the stacking of 5-NITP with the $n - 1$ template base stabilizes the indole rings in the same orientation established for a purine in the insertion site during physiological DNA synthesis.

Open Complexes Show DNA Untranslocated with the Single Stranded Template Stacking on W574. Open complexes depict 5-NIMP (Figure 5B,D) and dAMP (Figure 5C,D) opposite an abasic site untranslocated from the polymerase active site following release of the pyrophosphate. These structures resemble the previously published F_{18}•dAMP, crystallizing with four polymerase/DNA complexes per asymmetric unit and similar unit cell parameters (*11*). Also anticipated was a distribution of conformers due to switching of the primer from the polymerase to the exonuclease active site when a mispair is sensed. We observe in these new structures the distribution expected for complexes of RB69 gp43 exo− with DNA containing furan at the templating position, where two molecules adopt the polymerization conformation (MolA and MolC), one holds the primer terminus in the exonuclease active site (MolB), whereas the final complex is generally disordered (MolD). The only difference between F_{18}•dAMP and F_{21}•dAMP is the presence of three bases in F_{21}•dAMP appended to the 5′ end of the 18-mer template, and this longer template was used to observe additional interactions between the protein and single stranded 5′ template. The shorter 18-mer template leaves only two unpaired template bases after one cycle of nucleotide incorporation to the 14-mer primer (*11*).

The single stranded portion of these otherwise identical templates marks the only significant structural difference between the 18-mer and 21-mer open complexes. While in F_{18}•dAMP the two 5′ template bases stack between F359 and a beta hairpin loop found in the exonuclease domain (residues 253−261), the same portion of the 21-mer template in both F_{21}•dAMP and F_{21}•5-NIMP/5-NITP stacks on W574, before the additional bases exit into the solvent space. However, we note residual electron density peaks in difference ($F_o - F_c$) maps that indicate that the 5′ template also stacks on F359 with some discernible occupancy in these

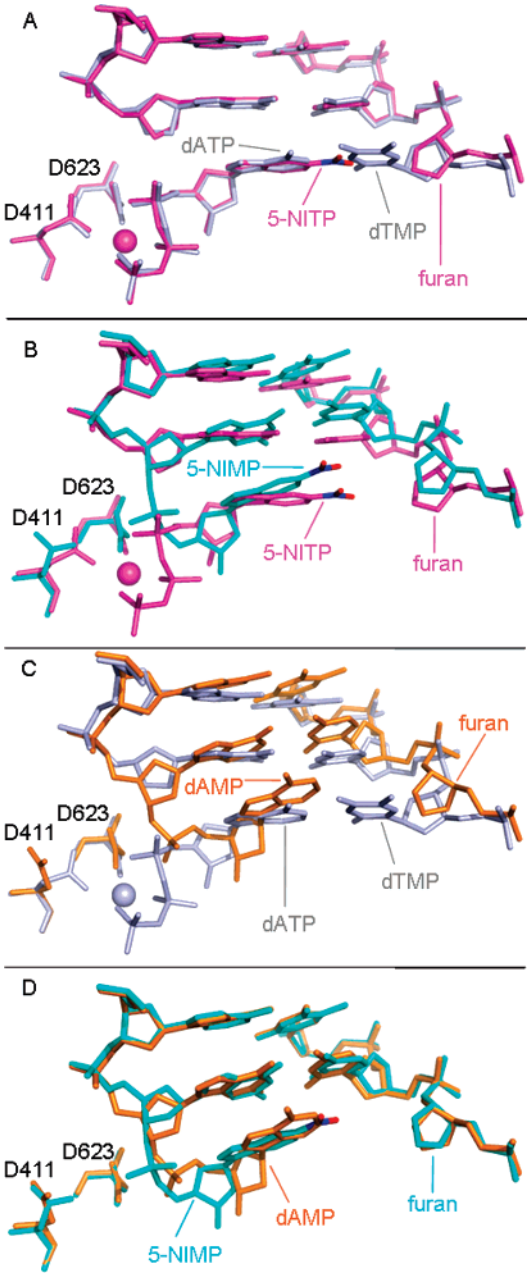

FIGURE 5: Structural superpositions of models in this study were created by alignment of α-carbons from the palm domain residues (383−468 and 573−729). A. Comparison of the two closed ternary complexes, F_{18}·5-NITP (magenta) and T_{18}·dATP (gray). The indole rings and the purine base are superimposable in the active site of the ternary complexes. The nitro group does not contact the furan template, but stacks with the template base at the $n - 1$ template position. B. F_{21}·5-NIMP/5-NITP (cyan) and F_{18}·5-NITP (magenta). After nucleotidyl transfer, 5-NIMP maintains the spatial relationship to the template·primer seen in the ternary complex with 5-NITP. This is evident by little movement of the deoxyribose sugar. C. F_{21}·dAMP (orange) and T_{18}·dATP (gray). Following incorporation into the primer strand opposite furan, dAMP does not approximate the orientation relative to the template·primer seen in the ternary complex with templating dTMP. The dAMP slides toward the template and into the major groove such that the deoxyribose sugars do not overlap in the superposition. D. Comparison of the open ternary and binary complexes, F_{21}·5-NIMP/5-NITP (cyan) and F_{21}·dAMP (orange). The adenine base slides toward the abasic site, distorting the DNA at the insertion site, while the 5-NIMP preserves geometry of the phosphate backbone. All superimposed bases are coplanar, showing that the DNAs are similarly oriented globally and have both forfeited the minor groove contacts near the active site. The DNA remain untranslocated in both structures.

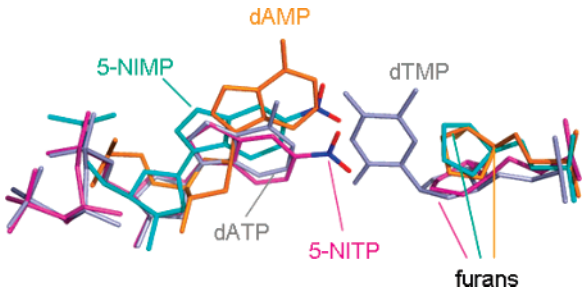

FIGURE 6: Close-up of the insertion site showing all superpositions from Figure 5 at once; dAMP is significantly different from the other three bases, having slid forward and into the major groove. This movement does not occur after incorporation of 5-NIMP, as is evident by the overlap of the deoxyribose from dATP, 5-NITP, and 5-NIMP.

new open complexes, suggesting an equilibrium between both orientations. In addition to F_{21}·dAMP and F_{21}·5-NIMP/5-NITP, T_{18}·dATP, F_{18}·5-NITP, an A_{18}·dTTP structure (PDB ID code: 1IG9) (*25*), and a thymine glycol binary complex (PDB ID code: 2DY4) (*28*) also exhibit similar stacking of the 5′ template on W574.

When Inserted Opposite an Abasic Site, 5-NIMP Does Not Significantly Distort the DNA Phosphate Backbone. When incorporated opposite an AP site, dAMP highly distorts the DNA by sliding toward the template and into the major groove, pulling the 3′ end of the primer away from the polymerase (Figure 5C). This phenomenon was observed in both F_{18}·dAMP (*11*) and F_{21}·dAMP, and occurs with an associated lack of translocation and loss of minor groove contacts with conserved residues K706 and Y567 in the proximity of the polymerase active site (*11*). When incorporated in the identical sequence context opposite a templating furan, 5-NIMP achieves a more favorable positioning such that the indole rings and nitro group approximate the relative local stacking orientation to the template·primer observed in the F_{18}·5-NITP closed ternary complex, resulting in little movement of the deoxyribose after chemistry as the fingers domain transitions from a closed to an open conformation (Figure 5B). However, this superposition of the F_{18}·5-NITP closed ternary complex with F_{21}·5-NIMP/5-NITP, its open counterpart, also shows that the template·primer in F_{21}·5-NIMP/5-NITP has tipped near the active site after nucleotidyl transfer, causing poor overlap for several base pairs exiting the active site (Figure 5B). This result shadows the comparison of the DNA from T_{18}·dATP with that of F_{21}·dAMP at all bases except for the newly incorporated dAMP (Figure 5C). Similar differences in the DNA between open and closed complexes were also noted previously (*11*) by comparing F_{18}·dAMP (open binary complex) to A_{18}·dTTP (closed ternary complex) (*25*). Accordingly, the preserved geometry of the phosphate backbone and deoxyribose with 5-NIMP at the primer terminus does not prevent disruption of minor groove contacts; the DNA in F_{21}·5-NIMP/5-NITP globally approximates that of the dAMP structures, untranslocated with DNA bases in identical planes, despite the significant differences between 5-NIMP and dAMP at the insertion sites (Figure 5D). Superimposing all four structures illuminates that furan·dAMP is more distorted than any base pair in this study (Figure 6), clearly demonstrating that dAMP experiences more displacement than 5-NIMP between open and closed complexes.

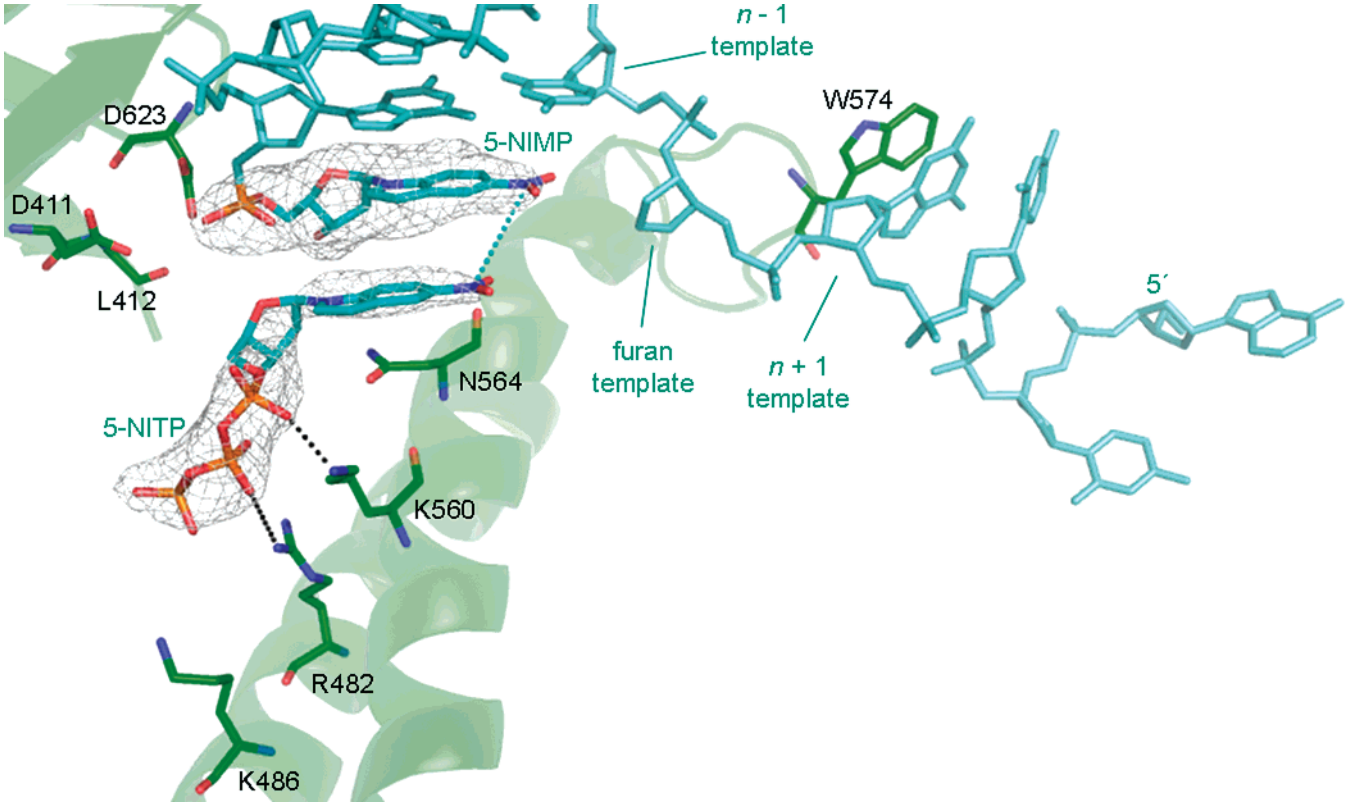

FIGURE 7: F_{21}•5-NIMP/5-NITP open ternary complex; 2.9 Å simulated annealing omit maps contoured at 4.5σ show 5-NIMP, untranslocated and incorporated at the primer 3′ end, and 5-NITP, bound to the fingers domain of this open complex. A possible 3.6 Å dipole−dipole interaction between the nitro groups is shown as cyan dashes, while salt bridges are shown in black. The $n + 1$ template base stacks on W574, and the additional three bases exit into the solvent space.

5-NITP Shows High Affinity for Stacking. Extraneous 5-NITP molecules stack at the 3′ end of the template strand in two of the four complexes of the F_{21}•5-NIMP/5-NITP crystal asymmetric unit (Supplementary Figure 1A, Supporting Information). These nucleotides, located on the DNA of MolC and MolD, each coordinate a Mg^{2+} ion and further validate the affinity of 5-NITP for stacking with nucleic acids. These molecules represent no obvious physiological function. When dATP is used in lieu of 5-NITP, difference ($F_o - F_c$) electron density map peaks are evident at the template 3′ end showing that dATP likely stacks at this same location in F21•dAMP, although the density is too weak to model the ligand. Also present was a single 5-NITP with the indole rings buried near T433, V436, N459, M461, and R581 in a pocket distant from the active site on the surface of the palm domain in MolA, with the deoxyribose encountering K435 (Supplementary Figure 1B). This third 5-NITP molecule also portrays no discernible physiological function.

5-NITP Binds Adjacent to the Active Site in the Open Ternary Complex. A fourth 5-NITP molecule in F_{21}•5-NIMP/5-NITP is located adjacent to the polymerase active site in MolC with the triphosphate tail stabilized via two salt bridges to K560 and R482 (Figure 7) and the indole rings positioned near residues F282, L561, and N564 (Figure 8). K560 and R482 contact nonbridging oxygens from distances of 3.0−3.3 Å, while N564 engages in van der Waals interactions with the ribose and base moieties of the nucleotide. The substituted nitro groups of the incorporated 5-NIMP in the polymerase active site and of this bound 5-NITP are separated by 3.6 Å, potentially allowing a weak dipole−dipole interaction to enable this propitious observation of

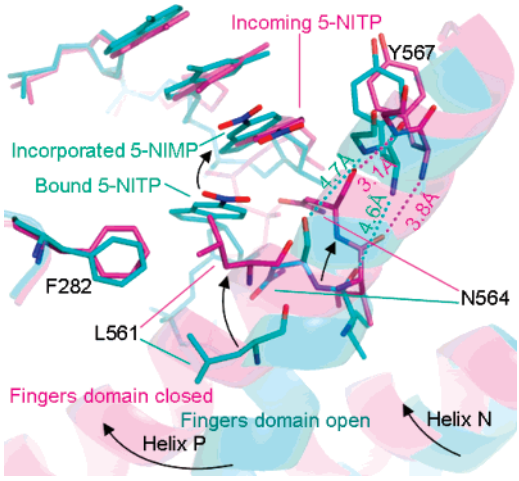

FIGURE 8: F_{21}•5-NIMP/5-NITP (cyan) and F_{18}•5-NITP (magenta) superposition. This diagram is a different view of Figure 5B, which emphasizes the movement of helices N and P. The 5-NITP indole rings bind to the open complex in pocket lined with F282, L561, and N564 at the hinge point that creates a discontinuity in helix P when the fingers open. As the fingers close, hydrogen bonds are restored in helix P between residues I563−Y567 and N564−G568. Upon formation of the closed complex, the bound 5-NITP molecule has moved into the active site and L561 occupies the nucleobase binding site. The leucine side chain of the closed complex overlaps with the 5-NITP of the open complex in this superposition, demonstrating necessity to relocate the bound substrate as the fingers close either into the active site or away from the protein into the solvent.

an initial dNTP binding event. While peaks are evident at the same location in the residual $F_o - F_c$ map for F_{21}•dAMP, electron density for an additional dATP is not adequate to

build the nucleotide, even though both complexes were cocrystallized with the same concentration of the incoming nucleoside triphosphate (2 mM).

DISCUSSION

Incorporation of 5-NITP opposite an abasic site represents a special case void of hydrogen bonding where RB69 gp43 approaches a catalytic rate rivaling those observed in forming normal Watson−Crick base pairs (*12*). This property designates 5-NITP as an ideal tool with which to study translesion DNA synthesis opposite an abasic site crystallographically, since inserting dAMP opposite an abasic site is much less kinetically favorable. In fact, previous efforts to crystallize a ternary complex with dATP opposite furan failed invariably without formation of the closed complex.

This work reveals that, opposite an abasic site, the nitro moiety of 5-NITP stacks with the $n - 1$ template base 3′ to the lesion (Figure 4), while conserving an orientation of the indole rings identical to that of the purine in a regular dTMP•dATP base pair (Figure 5A). The elevated rate of incorporation of 5-NITP appears to depend solely on the substituted nitro group, as Ind-TP (Figure 1D), though similarly hydrophobic to 5-NITP, possesses kinetic parameters very similar to those of dATP for incorporation opposite an AP site (*12*). This parallel underlines the stacking interaction we observe between 5-nitroindole and the $n - 1$ template base, suggesting that the permanent dipole on the nitro induces attractive forces that stabilize 5-NITP in the active site. The overlap of this nitro substituent with the N4−C4 bond of cytosine at the $n - 1$ template position could increasingly polarize the amine, which, in addition to holding 5-NITP in the active site with the appropriate geometry to support formation of the closed ternary complex, might compound stacking and stability of several template bases in the 3′ direction (*41*). Moreover, computational approaches have proposed a positive potential at the C5−C6 bond of cytosine in a CG base pair (*42*). While one oxygen from the nitro extends toward the N4 amine, the other oxygen nearly bisects the C5−C6 bond (Figure 4), possibly providing additional stabilization for the 5-nitroindole base. These observations in F_{18}•5-NITP strongly suggest that base stacking is the most important force influencing nucleotide incorporation opposite an AP site. With insertion of dATP opposite a nontemplating lesion, it is unlikely that the adenine base could interact with the $n - 1$ template base in the closed ternary complex without distorting the phosphate tail and Mg^{2+} ion significantly, which implies that base stacking with the nucleobase at the $n - 1$ primer position drives incorporation of dAMP opposite AP sites by B family polymerases.

Melting temperature experiments showed that thermodynamically 4-nitro and 6-nitro indole bases do not stabilize DNA as effectively as 5-NIMP when annealed opposite undamaged bases in the double helix, demonstrating the specificity of the stacking interaction with the nitro substituent at the 5 position (*18*, *43*). By considering the equivalent position in thymine, it is likely that altering the sequence at our $n - 1$ base from dCMP to dTMP in F_{18}•5-NITP would result in stacking between the nitro and the keto substituent of the C4. If the $n - 1$ base was changed to a purine, the nitro would instead be in proximity of the N7, orienting the nitro group to encounter a polar moiety in every case.

Loss of contacts between the protein and minor groove of the DNA due to distortions in the DNA double helix was thought to explain the untranslocated state of binary complexes where dAMP opposes a templating furan (*11*). Further hypotheses stated that these lost minor groove interactions signal the switching of the primer to the exonuclease active site for editing (*35*). We see now in the F_{21}•5-NIMP/5-NITP open ternary complex that chain termination opposite furan is possible without gross distortions of the primer at the insertion site. Our observations of 5-NIMP are consistent with the intrahelical positioning of dPTP opposite furan (PDB ID code: 1FZL) (*44*), where similarly no great distortion of the phosphate backbone is evident. Considering that both 5-NIMP and dPMP are chain terminators of DNA synthesis, unlike dAMP which can be bypassed to a limited extent (*13*), these data suggest that geometry about the insertion site is not the most significant factor that stalls RB69 gp43 exo− following incorporation of dAMP opposite furan.

Exploration of the incorporation characteristics of several dAMP isosteres demonstrated the importance of the adenine N1 and N3 for accurate DNA synthesis opposite dTMP by B family polymerases (*21*, *45*). One hypothesis put forth that the electron deficient Y567 ring interacts with the electron rich purine N3 during nucleotide incorporation, based on extrapolation of the A_{18}•dTTP (*25*) closed ternary complex where the incoming dTTP is near Y567. T_{18}•dATP allows verification of this expectation since the incoming nucleotide is a purine (dATP), and shows that the N3 is poised for van der Waals interactions with the tyrosine ring at a distance of about 4 Å. However, this interaction is apparently not needed for efficient incorporation of 5-NITP opposite a site of base loss, since the indole C7 in F_{18}•5-NITP lies in the same position as the adenine N3 in these closed ternary complexes (Figure 5A).

Running-start extension assays demonstrated the importance of the N3 for subsequent primer elongation after a purine isostere was incorporated at the primer 3′ end (*21*). While these extension assays do not inform the translocation state of unextended products, as does the crystal structure of 5-NIMP, a potentially necessary hydrogen bond is expected between K706 and the N3 of those adenine isosteres translocated to the $n - 2$ position by extension and an additional round of elongation. 5-NIMP does not contain an analogous N3, and therefore the hypothesis invoking K706 does not explain the chain terminating properties of hydrophobic bases, such as 5-NIMP, that remain stalled in the active site and never reach even the $n - 1$ position.

An additional difference between the closed ternary complexes T_{18}•dATP and A_{18}•dTTP is that the dATP structure contains a purine in the $n - 1$ primer position, where it is dideoxy chain terminated by ddGMP. The N3 of this guanine base shows stabilization from a water mediated hydrogen bond network in the minor groove near T622 (Figure 9). While the water molecule bound to this N3 was not modeled in A_{18}•dTTP, where ddCMP occupies the $n - 1$ primer, the difference map from the Electron Density Server (EDS) (*46*) shows a corresponding peak of 7σ. Across the duplex, the water mediated minor groove interactions at the $n - 1$ template and Y567 agree in both structures, although T_{18}•dATP orients dCMP in place of dGMP at this position. These observations suggest that the enzyme stabilizes the $n - 1$ base pair by water mediated interactions and

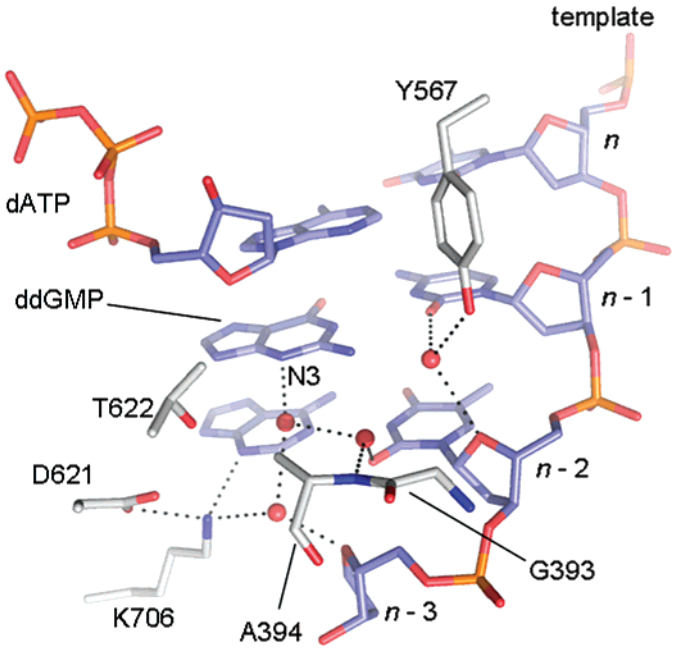

FIGURE 9: Hydrogen bonding in the minor groove of T_{18}•dATP. The $n - 1$ template (dCMP), Y567, and the O4′ of the $n - 2$ (dTMP) deoxyribose of the same DNA strand hydrogen bond with a water molecule. A different water molecule hydrogen bonds to the N3 of $n - 1$ primer (ddGMP). This water molecule is part of a larger hydrogen bonding network involving two additional water molecules, A394, D621, K706, and the $n - 1$ to the $n - 3$ base pairs. We observe equivalent water molecules in F_{18}•5-NITP.

without direct protein contacts (Figure 9), which could be a necessity of successful translocation and subsequent extension. A F•5-NIMP base pair would not be capable of establishing these interactions at the $n - 1$ position due to its hydrophobicity, where it would likely disrupt the hydrogen bonding network that links the $n - 1$ to the $n - 2$ and $n - 3$ base pairs (Figure 9). While the hydrophobicity of 5-NIMP possibly contributes to its action as a chain terminator, this should not influence insertion of 5-NITP, since it is known that there are no hydrogen bonds to the minor groove side of a base pair at the insertion site in B family polymerases (*25*).

Formation of the closed, catalytically competent conformation from the open conformation involves an approximately 60° rotation of helices N and P in the fingers domain (residues 469−572). The first ternary complex of RB69 gp43 exo− (PDB ID code: 1IG9) hinted that this motion allows the polymerase to shuttle the incoming nucleoside triphosphate into the active site by demonstrating the great distance traveled by R482, K468, and K560, the residues interacting with the triphosphate tail in that complex, from their relative positions in the apo structure (*25*, *31*). This movement of the fingers domain occurs about hinge points near the polymerase active site in both helices N and P. In the open complexes, this hinge exists as a discontinuity in the secondary structure of helix P where hydrogen bonds break between residues I563−Y567 and N564−G568 (Figure 8). Even though hydrogen bonding remains better preserved between open and closed complexes in helix N about its hinge, closure of the fingers domain causes similar gross scale movements in both helices to relocate the α-carbons of K560 (helix P) and R482 (helix N) a distance of 3−4 Å, while two helix turns away Y567 (helix P, Figure 8) (*47*) and I475 (helix N) remain nearly superimposable between binary and ternary complexes.

Kinetic observations of mutant enzymes provided evidence that the conserved residues K560 and R482 function in both dNTP binding and catalysis. K560A and R482A mutations not only accompany an increased K_d and depressed k_{pol} but also cease to exhibit a pre-steady-state burst in single-turnover experiments (*47*). Combined with the small elemental effect observed when adding dCTPαS (Sp + Rp) opposite a templating dGMP by K560A or R482A, this data demonstrates that a step before chemistry likely becomes rate limiting during catalysis by these mutants (*47*). Our structures support this data by illustrating that K560 and R482 bind the triphosphate tail in both the open (Figure 7) and closed (Figure 3) forms of the enzyme, which infers that these residues should alter both thermodynamic properties of binding and rate constants for chemical steps of polymerization. A similar kinetic trend holds for the N564A mutation, albeit to a lesser degree and without cessation of a pre-steady-state burst (*47*). While N564 stacks with the nucleobase rather than the triphosphate (Figure 8), we again see this residue contacting the dNTP in both open and closed conformations of the polymerase. Interestingly, K486A was characterized by markedly different kinetic parameters. While k_{pol} decreased, K_d remained approximately the same (*47*). K486 is unique from these other three conserved residues of the fingers domain in that it does not appear to contact the triphosphate in the open ternary configuration (Figure 7). These correlations between kinetics and structural observations convey the physiological relevance of the open ternary complex F_{21}•5-NIMP/5-NITP, showing that the bound 5-NITP is not simply a fortuitous interaction due to the tendency of this molecule to stack with nucleic acids and other 5-nitroindole bases.

We further note a rearrangement of interactions between these positively charged binding residues, R482 and K560, and the triphosphate tail. In the F_{21}•5-NIMP/5-NITP open ternary complex, K560 interacts with a nonbridging oxygen of the α-phosphate of 5-NITP, while R482 similarly contacts an oxygen of the β-phosphate (Figure 7). Upon formation of F_{18}•5-NITP, the dead-end ternary complex, the triphosphate has progressed past these residues such that K560 interacts with the bridging oxygen between the α- and β-phosphates, while R482 stabilizes nonbridging oxygens of the γ-phosphate (Figure 3).

The site of 5-NITP binding to the fingers domain in the open complex places the indole rings at the discontinuity of helix P, near residues F282, L561, and N564 (Figure 8). L561 also forms one side of the active site in the closed complex, and the mutation L561A accompanies reduced mismatch recognition by RB69 gp43 (*48*). This lessened fidelity might be a consequence of the increased volume of the mutant active site that better accommodates incorrect base pairs, although a second explanation implicates an increased range of movement at the neighboring triphosphate binding residue K560 (*48*). Visualizing the displacement of L561 as the fingers close between F_{21}•5-NIMP/5-NITP and F_{18}•5-NITP, we see that L561 pushes the indole rings of 5-NITP out of the adjacent binding site and toward the active site (Figure 8). Upon closure of the ternary complex, L561 occupies the adjacent nucleobase binding pocket where its side chain

would clash with the 5-NITP of the open complex (Figure 8).

Recent kinetics studies probing AP sites with synthetic nucleoside triphosphates demonstrated that K_d, the binding affinity of a nucleoside triphosphate, often correlates little with k_{pol}, the rate-limiting step of enzyme turnover (*49*). When compared to the large differences in k_{pol}, K_d varies only slightly between different synthetic nucleoside triphosphates, implying that a testing mechanism is at work, since each non-natural dNTP in solution possesses a similar affinity for binding regardless of its insertion rate. The F_{21}•5-NIMP/5-NITP structure supports an observed lack of base specificity inherent to K_d, depicting the $n + 1$ template base stacked on W574 where it cannot influence dNTP binding to helix P.

Closure of the fingers domain with a nucleotide bound to the open complex occurs with regard to the translocation state of the DNA and must produce one of two outcomes: the bound dNTP dissociates into solution as the fingers domain closes, or the dNTP enters the active site with the templating base intrahelical. Residues R482 and K560 push the substrate into the active site from the triphosphate tail, aided by L561 and N564 acting on the nucleobase (Figure 8). When the fingers domain closes, rotating and reestablishing the continuity of helix P, L561 comes to occupy the nucleobase binding site of the open complex. This necessitates movement of the bound dNTP away from L561. Successful relocation of the bound dNTP into the active site then either follows or coincides with translocation of the DNA, in order to avoid steric clash between the nucleotide and the primer terminus during migration of the nucleotide toward the active site. A second important aspect of translocation entails removal of the $n + 1$ template from its stacked position on W574 to an intrahelical orientation. Viewed as a whole synchronized process, closure of the fingers domain allows the enzyme to test a bound dNTP for favorable interactions with the template, bringing the bound dNTP and templating base together without forfeiting the option of dissociating the nucleotide.

CONCLUSION

Translesion DNA synthesis opposite abasic sites and subsequent bypass requires completion of two necessary tasks by the DNA polymerase prior to resuming template directed extension of the primer. First, the enzyme must choose a substrate for incorporation without cue from the template. Full bypass then presupposes translocation. The structures in this work indicate that base stacking likely plays a paramount role in the preferential incorporation of dAMP across an AP site, as this is the basis of efficient incorporation of 5-NITP. This supports experiments showing that neither steric fit nor hydrophobicity provides complete insight into the physical basis of the A-rule in B family polymerases (*12*, *21*). Moreover, our structural comparisons suggest that distorted geometry at the insertion site does not pose the greatest barrier in translocating a base opposite an AP site out of the active site to the $n - 1$ position. While 5-NIMP is superior to dAMP in chain terminating DNA synthesis opposite furan, 5-NIMP does not distort the primer terminus to the same extent as dAMP, calling into question the correlation between geometry at the insertion site and translocation state of the DNA.

We observed for the first time interactions between a B family DNA polymerase and a nucleoside triphosphate substrate, bound adjacent to the active site in a template independent manner. By capturing 5-NITP at three steps of incorporation opposite furan, we visualized RB69 gp43 exo− shuttling a nucleotide into the active site for insertion, correlating closure of the fingers domain with the transition of the dNTP from non base specific binding to direct interaction with the templating base in the active site.

ACKNOWLEDGMENT

We extend sincere thanks to Wendy Cooper for expression and purification of RB69 gp43 exo− and to Anthony J. Berdis, Matthew Hogg, and Mark A. Rould for providing insightful comments and suggestions during formulation of this manuscript. We acknowledge Stephen Corcoran, Ruslan Sanishvili, and Ward Smith from GM/CA CAT for their outstanding support during data collection at the APS.

SUPPORTING INFORMATION AVAILABLE

Supplementary Figure 1 showing a diagram of the 5-NITP molecules stacking on the template 3′ ends and bound to the surface of the palm domain. This material is available free of charge via the Internet at http://pubs.acs.org.

REFERENCES

1. Loeb, L. A., and Preston, B. D. (1986) Mutagenesis by apurinic/apyrimidinic sites, *Annu. Rev. Genet. 20*, 201−230.
2. Berdis, A. J. (2001) Dynamics of translesion DNA synthesis catalyzed by the bacteriophage T4 exonuclease-deficient DNA polymerase, *Biochemistry 40*, 7180−7191.
3. Goodman, M. F., Creighton, S., Bloom, L. B., and Petruska, J. (1993) Biochemical basis of DNA replication fidelity, *Crit. Rev. Biochem. Mol. Biol. 28*, 83−126.
4. Hatahet, Z., Zhou, M., Reha-Krantz, L. J., Ide, H., Morrical, S. W., and Wallace, S. S. (1999) *In vitro* selection of sequence contexts which enhance bypass of abasic sites and tetrahydrofuran by T4 DNA polymerase holoenzyme, *J. Mol. Biol. 286*, 1045−1057.
5. Shibutani, S., Takeshita, M., and Grollman, A. P. (1997) Translesional synthesis on DNA templates containing a single abasic site. A mechanistic study of the "A rule", *J. Biol. Chem. 272*, 13916−13922.
6. Lindahl, T. (1993) Instability and decay of the primary structure of DNA, *Nature (London, U.K.) 362*, 709−715.
7. Breen, A. P., and Murphy, J. A. (1995) Reactions of oxyl radicals with DNA, *Free Radical Biol. Med. 18*, 1033−1077.
8. Wallace, S. S. (1997) Oxidative Damage to DNA and Its Repair, in *Oxidative Stress and the Molecular Biology of Antioxidant Defenses* (Scandalios, J., Ed.) pp 49−90, Cold Spring Harbor Laboratory Press, Cold Spring Harbor, New York.
9. Schaaper, R. M., Kunkel, T. A., and Loeb, L. A. (1983) Infidelity of DNA synthesis associated with bypass of apurinic sites, *Proc. Natl. Acad. Sci. U.S.A. 80*, 487−491.
10. Evans, J., Maccabee, M., Hatahet, Z., Courcelle, J., Bockrath, R., Ide, H., and Wallace, S. (1993) Thymine ring saturation and fragmentation products: lesion bypass, misinsertion and implications for mutagenesis, *Mutat. Res. 299*, 147−156.
11. Hogg, M., Wallace, S. S., and Doublié, S. (2004) Crystallographic snapshots of a replicative DNA polymerase encountering an abasic site, *EMBO J. 23*, 1483−1493.
12. Zhang, X., Lee, I., and Berdis, A. J. (2004) Evaluating the contributions of desolvation and base-stacking during translesion DNA synthesis, *Org. Biomol. Chem. 2*, 1703−1711.
13. Zhang, X., Lee, I., and Berdis, A. J. (2005) A potential chemotherapeutic strategy for the selective inhibition of promutagenic DNA synthesis by nonnatural nucleotides, *Biochemistry 44*, 13111−13121.
14. Zhang, X., Lee, I., and Berdis, A. J. (2005) The use of nonnatural nucleotides to probe the contributions of shape complementarity and pi-electron surface area during DNA polymerization, *Biochemistry 44*, 13101−13110.

15. Reineks, E. Z., and Berdis, A. J. (2004) Evaluating the contribution of base stacking during translesion DNA replication, *Biochemistry 43*, 393−404.
16. Chiaramonte, M., Moore, C. L., Kincaid, K., and Kuchta, R. D. (2003) Facile polymerization of dNTPs bearing unnatural base analogues by DNA polymerase alpha and Klenow fragment (DNA polymerase I), *Biochemistry 42*, 10472−10481.
17. Gallego, J., and Loakes, D. (2007) Solution structure and dynamics of DNA duplexes containing the universal base analogues 5-nitroindole and 5-nitroindole 3-carboxamide, *Nucleic Acids Res*., in press.
18. Loakes, D., and Brown, D. M. (1994) 5-Nitroindole as an universal base analogue, *Nucleic Acids Res. 22*, 4039−4043.
19. Kim, T. W., and Kool, E. T. (2005) A series of nonpolar thymidine analogues of increasing size: DNA base pairing and stacking properties, *J. Org. Chem. 70*, 2048−2053.
20. Kool, E. T. (1998) Replication of non-hydrogen bonded bases by DNA polymerases: a mechanism for steric matching, *Biopolymers 48*, 3−17.
21. Beckman, J., Kincaid, K., Hocek, M., Spratt, T., Engels, J., Cosstick, R., and Kuchta, R. D. (2007) Human DNA polymerase alpha uses a combination of positive and negative selectivity to polymerize purine dNTPs with high fidelity, *Biochemistry 46*, 448−460.
22. Matray, T. J., and Kool, E. T. (1999) A specific partner for abasic damage in DNA, *Nature (London, U.K.) 399*, 704−708.
23. Kincaid, K., Beckman, J., Zivkovic, A., Halcomb, R. L., Engels, J. W., and Kuchta, R. D. (2005) Exploration of factors driving incorporation of unnatural dNTPS into DNA by Klenow fragment (DNA polymerase I) and DNA polymerase alpha, *Nucleic Acids Res. 33*, 2620−2628.
24. Doublié, S. (2006) Production of slenomethionyl proteins in prokaryotic and eukaryotic expression systems, *Methods Mol. Biol. 363*, 91−108.
25. Franklin, M. C., Wang, J., and Steitz, T. A. (2001) Structure of the replicating complex of a pol alpha family DNA polymerase, *Cell 105*, 657−667.
26. Takeshita, M., Chang, C. N., Johnson, F., Will, S., and Grollman, A. P. (1987) Oligodeoxynucleotides containing synthetic abasic sites. Model substrates for DNA polymerases and apurinic/apyrimidinic endonucleases, *J. Biol. Chem. 262*, 10171−10179.
27. Freisinger, E., Grollman, A. P., Miller, H., and Kisker, C. (2004) Lesion (in)tolerance reveals insights into DNA replication fidelity, *EMBO J. 23*, 1494−1505.
28. Aller, P., Rould, M. A., Hogg, M., Wallace, S. S., and Doublié, S. (2007) A structural rationale for stalling of a replicative DNA polymerase at the most common oxidative thymine lesion, thymine glycol, *Proc. Natl. Acad. Sci. U.S.A. 104*, 814−818.
29. Otwinowski, Z., and Minor, W. (1997) Processing of X-ray diffraction data collected in oscillation mode, in *Methods in Enzymology, Volume 276: Macromolecular Crystallography, Part A* (Carter, C. W., and Sweet, R. M., Eds.) pp 307−326, Academic Press.
30. Brunger, A. T., Adams, P. D., Clore, G. M., DeLano, W. L., Gros, P., Grosse-Kunstleve, R. W., Jiang, J. S., Kuszewski, J., Nilges, M., Pannu, N. S., Read, R. J., Rice, L. M., Simonson, T., and Warren, G. L. (1998) Crystallography & NMR system: A new software suite for macromolecular structure determination, *Acta Crystallogr., Sect. D: Biol. Crystallogr. 54*, 905−921.
31. Wang, J., Sattar, A. K., Wang, C. C., Karam, J. D., Konigsberg, W. H., and Steitz, T. A. (1997) Crystal structure of a pol alpha family replication DNA polymerase from bacteriophage RB69, *Cell 89*, 1087−1099.
32. Emsley, P., and Cowtan, K. (2004) Coot: model-building tools for molecular graphics, *Acta Crystallogr., Sect. D: Biol. Crystallogr. 60*, 2126−2132.
33. Murshudov, G. N., Vagin, A. A., and Dodson, E. J. (1997) Refinement of macromolecular structures by the maximum-likelihood method, *Acta Crystallogr., Sect. D: Biol. Crystallogr. 53*, 240−255.
34. Laskowski, R. A., McArthur, M. W., Moss, D. S., and Thornton, J. M. (1993) PROCHECK-a program to check the stereochemical quality of protein structures, *J. Appl. Crystallogr. 26*, 283−291.
35. Hogg, M., Aller, P., Konigsberg, W., Wallace, S. S., and Doublié, S. (2007) Structural and biochemical investigation of the role in proofreading of a beta hairpin loop found in the exonuclease domain of a replicative DNA polymerase of the B family, *J. Biol. Chem. 282*, 1432−1444.
36. Raghunathan, S., Kozlov, A. G., Lohman, T. M., and Waksman, G. (2000) Structure of the DNA binding domain of E. coli SSB bound to ssDNA, *Nat. Struct. Mol. Biol. 7*, 648−652.
37. DeLano, W. L. (2002) The PyMOL Molecular Graphics System, DeLano Scientific, San Carlos, CA.
38. Pelletier, H., Sawaya, M. R., Kumar, A., Wilson, S. H., and Kraut, J. (1994) Structures of ternary complexes of rat DNA polymerase beta, a DNA template-primer, and ddCTP, *Science (New York, N.Y.) 264*, 1891−1903.
39. Doublié, S., Tabor, S., Long, A. M., Richardson, C. C., and Ellenberger, T. (1998) Crystal structure of a bacteriophage T7 DNA replication complex at 2.2 A resolution, *Nature (London, U.K.) 391*, 251−258.
40. Steitz, T. A., and Steitz, J. A. (1993) A general two-metal-ion mechanism for catalytic RNA, *Proc. Natl. Acad. Sci. U.S.A. 90*, 6498−6502.
41. Saenger, W. (1984) *Principles of nucleic acid structure*, Springer-Verlag, New York.
42. Hunter, C. A. (1993) Sequence-dependent DNA structure. The role of base stacking interactions, *J. Mol. Biol. 230*, 1025−1054.
43. Loakes, D. (2001) Survey and summary: The applications of universal DNA base analogues, *Nucleic Acids Res. 29*, 2437−2447.
44. Smirnov, S., Matray, T. J., Kool, E. T., and de los Santos, C. (2002) Integrity of duplex structures without hydrogen bonding: DNA with pyrene paired at abasic sites, *Nucleic Acids Res. 30*, 5561−5569.
45. Hendrickson, C. L., Devine, K. G., and Benner, S. A. (2004) Probing minor groove recognition contacts by DNA polymerases and reverse transcriptases using 3-deaza-2′-deoxyadenosine, *Nucleic Acids Res. 32*, 2241−2250.
46. Kleywegt, G. J., Harris, M. R., Zou, J. Y., Taylor, T. C., Wahlby, A., and Jones, T. A. (2004) The Uppsala Electron-Density Server, *Acta Crystallogr., Sect. D: Biol. Crystallogr. 60*, 2240−2249.
47. Yang, G., Franklin, M., Li, J., Lin, T. C., and Konigsberg, W. (2002) Correlation of the kinetics of finger domain mutants in RB69 DNA polymerase with its structure, *Biochemistry 41*, 2526−2534.
48. Zhang, H., Rhee, C., Bebenek, A., Drake, J. W., Wang, J., and Konigsberg, W. (2006) The L561A substitution in the nascent base-pair binding pocket of RB69 DNA polymerase reduces base discrimination, *Biochemistry 45*, 2211−2220.
49. Zhang, X., Donnelly, A., Lee, I., and Berdis, A. J. (2006) Rational attempts to optimize non-natural nucleotides for selective incorporation opposite an abasic site, *Biochemistry 45*, 13293−13303.

BI7008807